

Total kinetic analysis reveals how combinatorial methylation patterns are established on lysines 27 and 36 of histone H3

Yupeng Zheng^{a,1}, Steve M. M. Sweet^{a,1,2}, Relja Popovic^b, Eva Martinez-Garcia^b, Jeremiah D. Tipton^a, Paul M. Thomas^a, Jonathan D. Licht^b, and Neil L. Kelleher^{a,b,3}

^aDepartments of Chemistry and Molecular Biosciences, Chemistry of Life Processes Institute, Northwestern University, Evanston, IL 60208; and ^bDivision of Hematology/Oncology, Robert H. Lurie Comprehensive Cancer Center, Feinberg School of Medicine, Northwestern University Chicago, IL 60611

Edited by James A. Wells, University of California, San Francisco, CA, and approved July 10, 2012 (received for review April 4, 2012)

We have developed a targeted method to quantify all combinations of methylation on an H3 peptide containing lysines 27 and 36 (H3K27-K36). By using stable isotopes that separately label the histone backbone and its methylations, we tracked the rates of methylation and demethylation in myeloma cells expressing high vs. low levels of the methyltransferase MMSET/WHSC1/NSD2. Following quantification of 99 labeled H3K27-K36 methylation states across time, a kinetic model converged to yield 44 effective rate constants qualifying each methylation and demethylation step as a function of the methylation state on the neighboring lysine. We call this approach MS-based measurement and modeling of histone methylation kinetics (M4K). M4K revealed that, when dimethylation states are reached on H3K27 or H3K36, rates of further methylation on the other site are reduced as much as 100-fold. Overall, cells with high MMSET have as much as 33-fold increases in the effective rate constants for formation of H3K36 mono- and dimethylation. At H3K27, cells with high MMSET have elevated formation of K27me1, but even higher increases in the effective rate constants for its reversal by demethylation. These quantitative studies lay bare a bidirectional antagonism between H3K27 and H3K36 that controls the writing and erasing of these methylation marks. Additionally, the integrated kinetic model was used to correctly predict observed abundances of H3K27-K36 methylation states within 5% of that actually established in perturbed cells. Such predictive power for how histone methylations are established should have major value as this family of methyltransferases matures as drug targets.

epigenetics | EZH2 | multiple myeloma | mass spectrometry | histone code

Several lysine residues in the tails of histones can be mono-, di-, or trimethylated from yeast to human. These position- and state-specific modifications have been implicated in many chromatin template activities (1). The critical roles of these modifications are further supported by their association with many physiological alterations and diseases (2–4). Genome-wide ChIP studies have provided extensive information regarding the localization of known histone methylation marks (5–7). However, this approach mainly captures snapshots of histone methylation. Therefore, it is unable to answer how methylation patterns are faithfully reestablished and maintained on newly synthesized or old histones to understand mechanisms of epigenetic inheritance (8, 9).

There are eight known histone methyltransferases (HMTs) targeting H3K36, including NSD1/2/3, SETD2, ASH1L, SETMAR, SMYD2, and SETD3 (10). Among them, MMSET (NSD2/WHSC1) preferentially methylates nucleosomal H3K36 and is capable of catalyzing the addition of as many as two methyl groups at this site (i.e., an H3K36 dimethylase) (11). By contrast, polycomb repressive complex 2 (PRC2) is the only known HMT for H3K27, consisting of four core subunits: EZH2 (catalytic subunit), EED, SUZ12, and RbAp48. Unlike the constitutively active H3K36 HMT, the catalytic activity of EZH2 is regulated by auxiliary subunits in the complex (12, 13).

A recent example highlights the great potential of linking methyltransferase kinetics with clinical malignancies. In vitro HMT assays indicated a recurring point mutation in EZH2 (Y641) identified in human B-cell lymphomas caused a reduction of enzymatic activity when unmodified substrate was used (loss of function as monomethylase) (4). However, subsequent kinetic analyses revealed the in vivo consequence of this heterozygous mutation is actually a gain of function, as the Y641 mutated form is a better H3K27 trimethylase and can produce higher levels of H3K27me3 when acting together with the WT allele (14).

The recurrent *t*(4;14) chromosomal translocation identified in 15% to 20% of patients with multiple myeloma (MM) leads to the overexpression of *MMSET* as a result of its fusion to an Ig gene with a strong promoter/enhancer (15). A pair of cell lines with high and low levels of MMSET were engineered from the MM patient-derived cell line, KMS11 (16). In the targeted KO (TKO) cell line, the translocated copy of MMSET was knocked out and overexpression of MMSET was lost. In the nontargeted KO (NTKO) cell line, the nontranslocated copy gene was knocked out and the expression level of MMSET remains high.

We and others have demonstrated the potential of stable-isotope labeling by amino acids in cell culture (SILAC)-based quantitative MS in investigating histone methylation dynamics (17–20). Here we report an extension of this method called MS-based measurement and modeling of histone methylation kinetics (M4K) and a general model for how H3K27 and H3K36 combinatorial methylation patterns are established in vivo. We forward this method and its resulting kinetic framework as an orthogonal, quantitative way to describe the histone code (21, 22).

Results

Quantitative, Multitarget MS. We developed a robust, multitarget MS assay for accurate quantification of combinatorial methylation of H3K27 and H3K36. It focused exclusively on the peptide K₂₇SAPATGGVKKPHR₄₀, liberated from H3 variants H3.1 and H3.2 by trypsin digestion (hereafter called H3K27-K36; *Materials and Methods*). We relied on a single amino acid difference in position 31 (Ala in H3.1/3.2 and Ser in H3.3) to exclude H3.3 without prefractionation. This H3K27-K36 peptide can harbor as many as 16 methylation combinations (four methylation states at

Author contributions: Y.Z., S.M.M.S., J.D.L., and N.L.K. designed research; Y.Z., S.M.M.S., R.P., E.M.-G., J.D.T., and P.M.T. performed research; Y.Z., J.D.L., and N.L.K. analyzed data; and Y.Z. and N.L.K. wrote the paper.

The authors declare no conflict of interest.

This article is a PNAS Direct Submission.

¹Y.Z. and S.M.M.S. contributed equally to this work.

²Present address: Genome Damage and Stability Centre, University of Sussex, Brighton and Hove BN1 9RQ, United Kingdom.

³To whom correspondence should be addressed. E-mail: n-kelleher@northwestern.edu.

This article contains supporting information online at www.pnas.org/lookup/suppl/doi:10.1073/pnas.1205707109/-DCSupplemental.

two sites, or 4^2), 15 of which are populated in vivo (Fig. 1A). Here, we used selected reaction monitoring (SRM) in a nanocapillary-liquid chromatography format on a triple quadrupole mass spectrometer to develop and validate a quantitative assay (Fig. 2C and Fig. S1). This assay platform was able to quantify all species from combinatorial methylation of the H3K27-K36 peptide in a single LC run. Transitions for the K27me3-K36me3 species were also created; however, this species was never detected, consistent with other reports (23, 24).

To validate this platform further, we compared the methylation of NTKO vs. TKO cell lines. The level of H3K36me2 is increased with a concomitant decrease of H3K27me2/3 in the MMSET-overexpressing NTKO cells (Fig. 1B), in agreement with our previous results with the larger 1–50 piece of H3 (3). The combinatorial methylation patterns from our MS assay show that K27me1-K36me2 is the dominant species in NTKO (accounting for 60% of the total signal) whereas K27me1-K36me2 and K27me2-K36me0 are the two major species in TKO cells (accounting for 18% and 29%, respectively; Fig. 1A and Table S1). Others have used this type of triple-quadrupole MS platform, which has $>10^4$ dynamic range and the ability to quantify >200 analytical targets in a single run (25), for studying changes in histone modifications (26–28). We next sought to extend this method to all stable-isotope states of the H3K27-K36 peptide created by SILAC (29). In our implementation, we use heavy-Arg ($^{13}\text{C}_6$) and heavy-Met ($^{13}\text{C}_1^2\text{H}_3$; Fig. 2A). This dual-labeling procedure creates a high number of “SILAC intermediates,” but can distinguish old from new histones, and both old and new methylation events on each of them (Fig. 2, Right) (19).

Measurement of 99 SILAC Intermediates of H3K27-K36 in a Single LC-MS Run. In our dual-label SILAC approach, cells were grown in media containing heavy arginine and heavy methionine for four generations to achieve $>90\%$ incorporation (Fig. 2A). Then, cells were released into unlabeled (i.e., light) media (Fig. 2B). Peptides

labeled with heavy arginine are from old histones synthesized before release, and those with light arginine are from histones synthesized after release. Similarly, heavy methyl groups represent old methylation and light methyl groups new methylation (i.e., heavy is old and light is new). Because as many as three methyl groups can be incorporated on each lysine and a mixture of old and new methyl groups can be generated for each, we use a nomenclature to convey both the methylation state and the number of methyl groups that are heavy (Fig. 2, Right) (20). Because there are 10 possible forms for one methylation site in old histones (0:0, 1:1, 1:0, 2:2, 2:1, 2:0, 3:3, 3:2, 3:1, and 3:0), there are 10^2 or 100 theoretical combinations of SILAC intermediates for the two methylation sites in the old H3K27-K36 peptide. From the 100 intermediates, only 84 were monitored because 16 derive from K27me3-K36me3 and were therefore not detectable.

New H3K27-K36 should display only 15 species, assuming no contamination from a pool of heavy Met (or *S*-adenosyl methionine) after the media switch (Fig. 2A vs. Fig. 2B). In new histones, new monomethylation from the pool of old, heavy Met (or *S*-adenosyl methionine) contributed only 0.7% and 3.4% of overall monomethylation at K27 and K36, respectively (Fig. S2D; further explanation is provided in *SI Text, Section 3*). Therefore, only 15 SILAC species from new histones were monitored to increase data quality for each of the total 99 SILAC intermediates of the H3K27-K36 peptide. In addition, two criteria have been adopted to ensure the overall data quality (*SI Text, Section 1*).

Kinetic Modeling. Simultaneous measurement of methylation kinetics for K27 and K36 allows us to study cross-talk between these two sites. However, analyzing the kinetic behavior of individual SILAC intermediates provides only suggestive trends for selected cases (*SI Text, Section 2*). To take into account all the concentration changes together when the growth media is switched, we built a model containing a total of 44 rate constants to capture the interconversion of 84 SILAC intermediates by sequential methylation and demethylation steps (Fig. S3 and *SI Text, Section 4*). For the modeling step of the M4K workflow (Fig. 2D), we focused on the interconversion of methylated states for old histones because this removed the complication of new histone synthesis depicted in the full kinetic model of Fig. S4. As shown in Fig. 2D, two assumptions are made for this system: (i) the relative levels of each SILAC intermediate can be taken as a concentration, and (ii) sequential methylation and demethylation can be described by reversible first-order kinetics (*SI Text, Section 8*). The final output of the M4K process is a set of rate constants (Fig. 2E) we call neighboring-site methylation-dependent effective rate constants (NMDERCs), or simply “effective rate constants.” We use the word “effective” to emphasize that they are compound rate constants related to k_{cat} by the scalar $[E]/K_m$ and represent a complex set of in vivo processing events including the joint action of many methyltransferases and demethylases in the highly structured and dynamic environment of the nucleus. NMDERCs were generated by solving ordinary differential equations (ODEs) with a least-square fitting approach as described previously (20). In sum, we determined 44 effective rate constants for H3K27-K36 from old histones by using 84 measured concentrations of intermediate species (Figs. 2E and 3). The effective rate constants are reported as means of all the values from solution sets populated by 5,000 computations that have a goodness of fit (measured as rmsd) within 25% of the minimum. Here, these solution sets were between 2,700 and 3,000 of the 5,000 computations. Values for the SD derived from this filtered solution space were also determined and are reported inside parentheses following each of the 44 average effective rate constants (Fig. 3). Collections of effective rate constants (with units of d^{-1}) solved by M4K can explain the kinetic behavior of multiple SILAC intermediates (examples are provided in *SI Text, Section 5*).

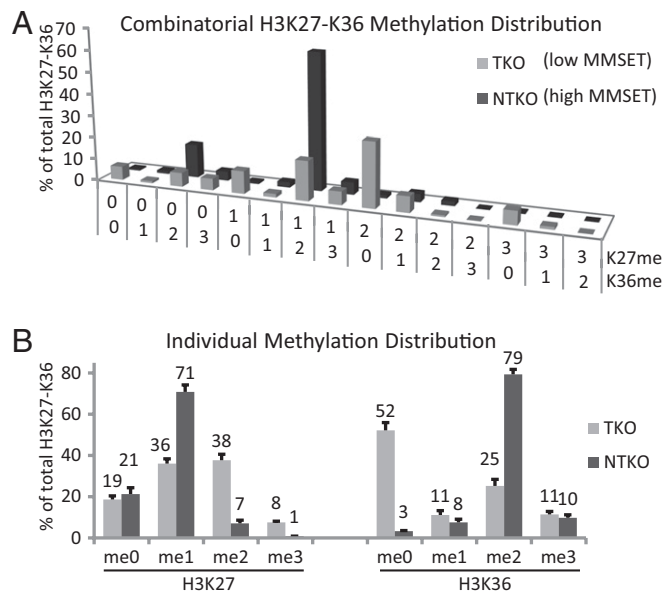


Fig. 1. Increase of H3K36me2 with concomitant decrease of H3K27me2/3 in NTKO cells that overexpress the MMSET methyltransferase. (A) Abundance distribution of all 15 detectable species from combinatorial methylation of the H3K27-K36 peptide in unlabeled TKO and NTKO cells measured by SRM using a nanocapillary triple quadrupole LC-MS platform. (B) Individual K27 and K36 methylation distributions were further calculated by summing the appropriate data channels corresponding to each particular site ($n = 8$; error bars indicate \pm SD).

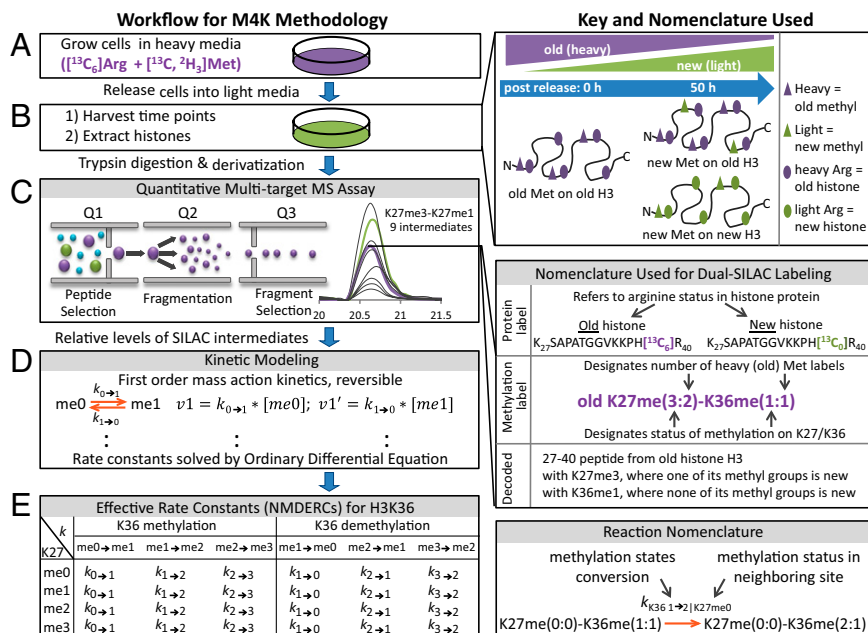


Fig. 2. Schematic of experimental workflow for the integrated M4K approach, which involves dual-label SILAC labeling to detect old and new methylation events on old vs. new histones. The M4K workflow begins with exhaustive labeling of cells on heavy media (A), followed by media exchange (B), quantitative MS analysis of as many as 99 SILAC intermediates (C), and kinetic modeling (D) to determine effective rate constants (E).

Di- or Trimethylation of K36 or K27 Antagonizes Methylation Rates at the Other Site. As shown in Fig. 3A, the effective rate constants are 2.20 and 1.00 d⁻¹ for formation of K27 mono- and dimethylation, respectively (i.e., K27me0→1 and K27me1→2), when the methylation status at K36 is unmodified (Fig. 3A, first row, first two columns). When K36me1 is present, these rate constants have quite comparable values of 3.5 and 1.2 d⁻¹ (Fig. 3A, blue text). However, when K36me2 or K36me3 is present, these rate constants decrease by approximately fivefold (in the case of K27me0→1) and 50 to 100 fold (in the case of K27me1→2; Fig. 3A, Left, red text). Similar decreases of rate constants (ranging from 5 to 100 fold) were also observed for formation of K36me1 and K36me2 when the methylation status at K27 was di- or trimethylated (Fig. 3A, Right, green vs. red text). Note again that the

greatest antagonism was found in the rate constants for the formation of dimethylated species when the other site was di- or trimethylated. We call this effect “bidirectional antagonism” to summarize the nature of this two-way, negative cross-talk between the higher methylation states of H3K27 and H3K36. This is consistent with observations in the data [e.g., that appearance rates of selected SILAC intermediates containing K27me(2:1) or K36me(2:1) decreased when the other site is di- or trimethylated; Fig. S5 B and C]. Our findings are also in agreement with the previously reported one-way antagonism reported in vitro whereby EZH2 is unable to methylate K27 in the presence of K36me2/3 (13, 23).

MMSET Overexpression Disrupts Normal Rates of Methylation and Demethylation at K27 and K36. To understand how the MMSET-induced increase in H3K36me2 causes the decrease of H3K27me2/3

Effective Rate Constants Determined by M4K

A TKO (low MMSET)

K36 status	K27 methylation			K27 demethylation			K27 status	K36 methylation			K36 demethylation		
	me0→1	me1→2	me2→3	me1→0	me2→1	me3→2		me0→1	me1→2	me2→3	me1→0	me2→1	me3→2
me0	2.20 (0.035)	1.00 (0.0083)	0.05 (0.0022)	0.21 (0.033)	0.07 (0.011)	0.02 (0.037)	me0	1.0 (0.052)	7.2 (0.31)	0.73 (0.0099)	0.04 (0.22)	0.6 (0.16)	0.3 (0.088)
me1	3.5 (0.33)	1.2 (0.30)	0.04 (0.024)	1 (1.0)	0.1 (0.056)	0.1 (0.11)	me1	0.3 (0.027)	4 (0.98)	0.14 (0.0033)	0.02 (0.12)	0.13 (0.032)	0.05 (0.043)
me2	0.53 (0.016)	0.01 (0.013)	0.1 (0.19)	0.08 (0.031)	0.4 (0.44)	1 (4.1)	me2	0.06 (0.0016)	0.05 (0.037)	0.3 (0.26)	0.3 (0.065)	0.1 (0.17)	1 (1.9)
me3	0.16 (0.0073)	0.02 (0.017)	ND	0.08 (0.045)	0.2 (0.58)	ND	me3	0.06 (0.024)	0.2 (0.26)	ND	0.2 (0.24)	4 (8.5)	ND

B NTKO (high MMSET)

K36 status	K27 methylation			K27 demethylation			K27 status	K36 methylation			K36 demethylation		
	me0→1	me1→2	me2→3	me1→0	me2→1	me3→2		me0→1	me1→2	me2→3	me1→0	me2→1	me3→2
me0	14 (1.2)	2 (0.56)	0.2 (0.15)	15 (1.7)	0.2 (0.35)	0.1 (0.21)	me0	15 (0.73)	19 (1.2)	0.19 (0.0049)	0.3 (0.73)	0.09 (0.059)	0.01 (0.031)
me1	9 (0.74)	2 (0.79)	0.3 (0.33)	9 (2.2)	0.2 (0.49)	0.4 (1.1)	me1	9 (0.90)	22 (4.0)	0.04 (0.0014)	6 (1.1)	0.2 (0.011)	0.01 (0.017)
me2	1.08 (0.0025)	0.01 (0.0036)	0.04 (0.073)	0.01 (0.011)	0.03 (0.065)	6 (5.3)	me2	0.6 (0.21)	0.2 (0.11)	0.05 (0.082)	0.3 (0.20)	0.02 (0.047)	2 (5.9)
me3	0.4 (0.045)	0.03 (0.050)	ND	0.08 (0.018)	2 (4.1)	ND	me3	0.5 (0.61)	0.6 (0.83)	ND	1 (1.5)	0.3 (0.87)	ND

Fig. 3. Effective rate constants determined by M4K for (A) TKO cells with low MMSET levels and (B) NTKO cells with high levels of the MMSET methyltransferase. NMDERCs were estimated by solving ODEs. All the effective rate constants are reported as an average of values emerging from a solution space in which each value is within 25% of a minimum rmsd determined in 5,000 computations. Values for the SD derived from this solution space were also determined and are reported inside the parentheses.

(Fig. 1 and Table S1), histones from MMSET-overexpressing NTKO cells were subjected to M4K analysis. The patterns of changes in effective rate constants from NTKO cells (Fig. 3B) were very similar to the decreases found in TKO cells [compare rate constants in blue (K27) or green (K36) vs. those in red for the di- or trimethylated species for the antagonistic site]. The rate constants for formation of monomethylated species were reduced by ~9 to 50 fold and values for formation of di-methylated species were decreased by ~50 to 100 fold by the presence of di- or trimethylation at the adjacent site.

In NTKO cells with high MMSET levels, the effective rate constants for formation of K36 mono- and dimethylation were 15 and 19 d^{-1} and 9 and 22 d^{-1} , respectively (when K27me0 or K27me1 was present; Fig. 3B, Right, first two rows). Significant increases ranging from threefold to more than 30-fold were observed compared with the analogous values in MMSET-low TKO cells (Fig. 3A vs. Fig. 3B, green text, increases underlined). In other words, conversion of K36me0 to K36me1 and K36me1 to K36me2 is much faster in MMSET-high cells. This was not true for K36me2 processing to K36me3. The lack of increase in effective rate constants for K36 trimethylation indicates that MMSET indeed serves as a H3K36 dimethyltransferase *in vivo*. This result is consistent with a previous report obtained by an HMT assay using nucleosome substrates *in vitro* (11), and by our own (3) and other previous work (30). Importantly, this result from a known perturbation of MMSET validates our overall measurement and modeling approach, M4K.

Another notable change was found in NTKO vs. TKO cells by comparing effective rate constants for K27 methylation and demethylation in these two cell types. In the presence of high levels of MMSET, both were greatly increased for monomethylation and slightly increased for dimethylation (i.e., $me0 \leftrightarrow$ and $me1 \leftrightarrow 2$), when K36me1 or K36me2 was present (Fig. 3A, Left, first two rows, vs. Fig. 3B, blue text, increases underlined). Approximately two- to sixfold increases were found in rate constants corresponding to formation of K27me1 from K27me0 (i.e., methylation), along with 18- to 71-fold increases for those corresponding to formation of K27me0 from K27me1 (i.e., demethylation).

Effective Rate Constants for Old and New Histones Are Similar. Given that the rate constants determined were for old histones, we decided to test whether this matrix of 44 values could also be applied to new histones. We first used the matrix of rate constants from Fig. 3A to predict the methylation status of old histones (Fig. S6B). We then used experimental values for new histone synthesis and dilution (Fig. S2B and SI Materials and Methods) to run a simulation that leads to predicted values for all 15 H3K27-K36 methylation species from new histones (Fig. S6D). When compared on a K27 or K36 site-specific basis, the predicted methylation levels in old and new histones (Fig. S6B and D) are very similar to those observed (Fig. S6A and C). This suggests that HMTs treat old and new histones in the same way. At first, this would seem to contradict the observation that the rate of new methylation on new histones at H3K27 and H3K36 is faster than that for old histones (Fig. S6A and C). This apparent paradox can be explained by the fact that, in old histones, H3K27 and H3K36 are extensively methylated, limiting the availability of the favorable substrates (me0 and me1). However, for new histones, H3K27 and H3K36 are not extensively methylated and therefore offer high concentrations of favorable substrates for HMTs. It was previously reported that the rate of methylation of H3K79 was similar for old and new histones (19). Old H3K79 shows far lower levels of basal methylation (~90% unmodified); hence, old histones present large concentrations of favorable substrate (K79me0). We therefore believe that the difference in appearance rate of new methylation at H3K27 or H3K36 in old and new histones is simply caused by different substrate concentrations

instead of distinct regulatory mechanisms for the pools of old vs. new histones.

Modeling Methylation Levels in Perturbed Systems. To perturb the methyltransferase activity of MMSET, we overexpressed truncated MMSET lacking its fourth PHD domain (MMSET-PHD4) in TKO cells. The levels of methylation at K27 and K36 were then measured in TKO cells overexpressing an empty vector, full-length MMSET, or MMSET-PHD4 (Fig. 4A). MMSET-PHD4 can still drive some increase in K36me2 levels, but the loss of K27me2/3 was not as great as that observed with full-length MMSET (Fig. 4A). This suggests that deletion of the PHD4 domain compromises, to some extent, the HMT activity of MMSET. This is consistent with the model of bidirectional antagonism introduced earlier. Because the levels of K36me2 are reduced by the hindered K36 HMT, the K27 HMT can methylate more K27 before antagonism by K36me2 slows down its action. As a result, more K27me2 is established when MMSET-PHD4 is expressed relative to full-length MMSET. To further test this theory quantitatively, we used our kinetic model and now-known set of effective rate constants. We decreased the effective rate constants for formation of K36me1 and K36me2 to be between those found for the MMSET-low and -high cells. As shown in Fig. 4B, the final abundance values for methylation states at K27 and K36 from a simulation using these altered effective rate constants recapitulated the observed methylation levels to within 5% for TKO with MMSET-PHD4 expression (TKO-MMSET-PHD4). It is also possible that demethylation at K27 is reduced in the absence of the PHD4 domain. This alternative mechanism could also act to explain the reduced loss of K27me2/3 observed in TKO cells expressing MMSET-PHD4 vs. MMSET.

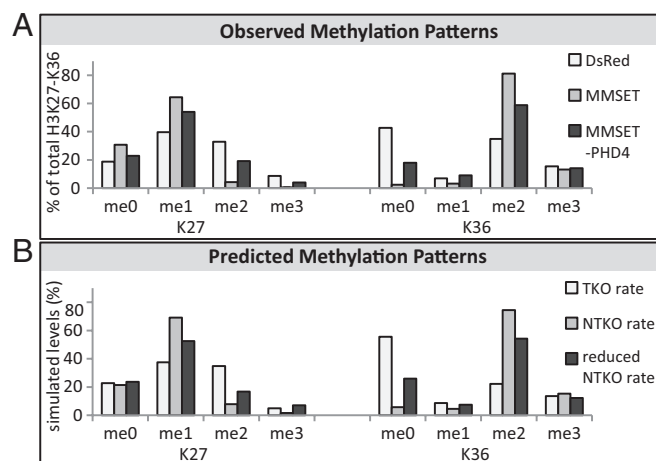


Fig. 4. Use of the kinetic model to predict methylation levels. (A) Relative levels of H3K27 and H3K36 methylations observed in TKO cells from add-back experiments ($n = 3$ technical replicates). DsRed, empty vector; MMSET, vector with full length MMSET; MMSET-PHD4, vector with PHD domain 4 deletion of MMSET. (B) Simulation results based on a full kinetic model depicted in Fig. S4. The matrix of effective rate constants from TKO cells (Fig. 3A) and NTKO cells (Fig. 3B) were used to simulate methylation levels observed in DsRed cells (TKO rate) and MMSET cells (NTKO rate), respectively. The NTKO rate constants with values for formation of H3K36me1 and H3K36me2 were set as four and two times the analogous values in TKO, respectively, to simulate MMSET-PHD4 (reduced NTKO rate). Relative levels of 15 methylation species in unlabeled TKO cells (Table S1) were used as initial concentration. Dilution rate constant is equal to the synthesis rate constant of $0.304 d^{-1}$ (determined for TKO cells; SI Materials and Methods).

Discussion

Competition for Favorable Substrates Determines Combinatorial Methylation Patterns *In Vivo*. Taking the kinetic rules specified by the effective rate constants, this work provides a basis for understanding how methylation patterns on new histones are established. Starting from 10 hypothetical H3 molecules, newly synthesized and without any methylation (Fig. 5, *Left*), the effective rate constant in TKO cells for the formation of monomethylation in K27 is greater than that of K36 (when the other site is me0). Therefore, more K27me1 than K36me1 would be formed from unmodified H3 (Fig. 5A, second column). On the contrary, the effective rate constant for the formation of dimethylation in K27 is less than that of K36 (when the other site is me1); therefore, in H3 with K27me1 and K36me1 marks, most methylation would occur in K36, resulting in K36me2 being formed preferentially vs. K27me2 (Fig. 5A, third column). When K36me2 has formed, it greatly slows the methylation of K27 (Fig. 5A, fourth column); eventually, more K27me1 molecules become K27me2 (Fig. 5A, third column) and antagonize the additional methylation in K36 (Fig. 5A, fourth column). The formation of trimethylation on either site is slow (Fig. 5A, fifth column). In MMSET-overexpressing NTKO cells, the formation of K36me1 and me2 becomes much faster than the methylation rate of K27. As shown in the third column in Fig. 5B, the HMT for K27 lags behind the hyperactivity of HMTs for K36. This leads to K36me2

forming preferentially and sharply reduces progressive methylation at K27 on the same H3 tail.

Overall, H3 molecules in the left three columns in Fig. 5 are referred to as favorable substrates, as the methylation rates for K27 and K36 are fairly fast. By contrast, molecules in the right two columns in Fig. 5 are referred to as unfavorable substrates, as methylation rates for species with di- or trimethylation slow greatly. It is worth emphasizing that bidirectional antagonism is very similar between TKO and NTKO cells as specified by effective rate constants in Fig. 3, with quite similar factors observed for reductions in the analogous rate constants in the two systems. The very different methylation patterns observed in TKO and NTKO cells appear to be determined in large part by the methylation “race” between K27 and K36 to reach a dimethylated state, which can lower the rate of further methylation at the other site by a factor of ~100 (Fig. 3). It will be interesting to see how general these results are across different cell types.

From Kinetics to Mechanism. Recent *in vitro* data showed K36 methylation was unaffected by K27 methylation state, whereas K27 methylation was inhibited by K36me2/3 (13, 23). The antagonism of K27 methylation by K36me2/3 is observed in both *in vitro* and our *in vivo* studies, and likely reflects an intrinsic property of the PRC2 complex despite the yet unidentified biochemical mechanism. On the contrary, the antagonism of K36 methylation by K27me2/3 is not likely to be a property of the methyltransferase itself. Several mechanisms can be envisaged for the inhibition of K36 methylation in the presence of K27me2/3. For instance, higher-order chromatin compaction as a result of K27me2/3 could render histones inaccessible to K36 HMTs. It is apparent that one-way antagonism is not enough to account for the observed low levels of hypermethylated H3K27-K36 species carrying a total of five or six methyl groups (i.e., K27me2-K36me3, K27me3-K36me2, or K27me3-K36me3). This is further demonstrated by overestimation of levels of di- and trimethylation in K27 and K36 when bidirectional antagonism is not considered, whereby each site is modeled independently by using a subset of effective rate constants (Fig. S7B and C and *SI Text, Section 6*). By contrast, invoking two-way antagonism accounts for H3K36 HMTs not continuously methylating H3 in the presence of K27me2/3 to form such hypermethylated species. Besides limiting the formation of these hypermethylated species, it is also very likely that demethylation is important in reversing the formation of these species (*SI Text, Section 7*).

One of the intriguing findings in this study is the increase of K27 methylation and demethylation rate constants in cells with elevated MMSET levels in the context of chromatin with unmodified or monomethylated K36 (Fig. 3A vs. Fig. 3B, rate constants in blue). As EZH2 is the major K27 HMT, it suggests that the activity or the concentration of EZH2 may be altered in myeloma cells. As a result of the involvement of EZH2 in multiple oncogenic processes (31), the mechanism of this increase in the rate of K27 methylation turnover is worth further investigation. An explanation informed from the kinetic results here would recognize that, with “overloaded” amounts of MMSET to drive methylation at K36 to me2, the existing pool of EZH2 is free to drive higher rates of K27 methylation at K36me0/1-containing chromatin without an increase in its total nuclear concentration. Similarly, the increase of K27 demethylation rate could be caused by increased activity of K27 demethylase(s), a greater global concentration in nuclei, or a larger effective concentration at specific loci. However, further research is required to reveal the biochemical mechanisms underlying these interesting kinetic observations.

Methylation Rate Constants Determined by HMT Assays *In Vitro* and M4K *In Vivo*. As shown in Fig. S7A, when the nuclear concentration of EZH2 is assumed to be 10 nM, our estimation of its catalytic efficiencies are close to the values measured by HMT assays

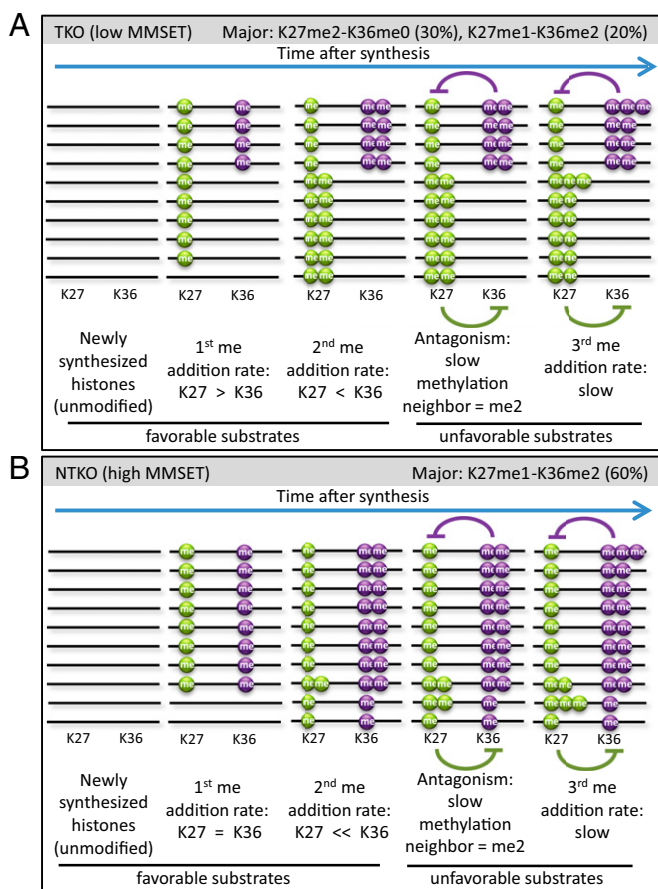


Fig. 5. Qualitative model depicting the competition between K27 and K36 HMTs for favorable substrates by bidirectional antagonism and slow trimethylation determines the combinatorial methylation patterns in TKO and NTKO cells. The schematic highlights the processing likely to occur for 10 newly synthesized H3 molecules with unmodified K27 and K36 residues (far left) for TKO cells (A) and NTKO cells (B).

in vitro (14). It has been demonstrated recently that the methylation pattern of H3K27 in vivo is determined by the preference of EZH2 for substrate with less methylated H3K27 (31). This intrinsic property of EZH2 can be described by catalytic efficiency ratio of the different substrates in vitro (H3K27me0:me1:me2 ratio of 9:6:1) (31), which was also captured by M4K for endogenous substrates ($k_{me0 \rightarrow 1}:k_{me1 \rightarrow 2}:k_{me2 \rightarrow 3}$ ratio of 44:20:1).

M4K and MS Technology in Epigenetics. In retrospect, the aforementioned cross-talk between two histone marks can only be discovered when both of them are measured simultaneously. Therefore, MS measurements of a peptide containing all marks of interest are critical to achieve for determination of interdependent arrays of effective rate constants. Therefore, “middle-down” or “top-down” MS approaches that can resolve old and new histone and old and new methylation on 5.3-kDa [1–50 piece of H3 (32)], 2.4-kDa [1–23 piece of H4 (33)], or even 15-kDa (full-length H3) present one way forward. Notably, any MS approach measuring bulk histones does not typically detect species below 0.01%. Therefore, local exceptions to the kinetic trends reported here could be possible at specific loci in the genome.

Predictive Power of Quantitative Modeling for Understanding Writing and Erasing of Histone Code. We expect that our qualitative and quantitative models could be applied to other systems with different H3K27 or H3K36 HMT perturbations. The complete kinetic model should provide quantitative guidance for development and application of methyltransferase or demethylase inhibitors to restore aberrant H3K27 and H3K36 methylation in disease. Finally, the M4K technology can be extended to analyze other combinatorial methylations in histones and other proteins.

Materials and Methods

Cell Culture, SILAC, and Sample Preparation. KMS11 TKO and NTKO cells (16) were cultured for 8 d at 37 °C in heavy RPMI media (customized double

omission; AthenaES) supplemented with [¹³C₆]Arg and [¹³C₁,²H₃]Met (Cambridge Isotope Laboratories) and 10% dialyzed FBS before release into unlabeled RPMI media with 10% dialyzed FBS. Cells were harvested at 0, 5, 10, 25, and 50 h after the media switch. Acid-extracted histones were derivatized by using propionic anhydride and digested with trypsin as described previously (34) (*SI Materials and Methods*).

MMSET Overexpression. TKO cells were transduced for 2 d with retroviral vectors harboring MMSET or MMSET deleted for the C-terminal PHD domain. All retroviruses were produced by transfection of amphotropic 293T cells with plasmids and FuGene 6 (Roche) according to the manufacturer's protocol. Infected cells were sorted by using DsRed and further expanded before studies.

SRM Detection of H3K27-K36. SRMs capable of discriminating all 15 H3K27-K36 methylation species were developed with three fragment ions for each species. Data were analyzed in Skyline with Savitzky–Golay smoothing (35). All SILAC intermediates from each H3K27-K36 methylation species were grouped as a whole for manual peak determination to avoid bias. Total areas from two fragment ions were used for quantification. Few cases of channel contaminations caused by overlapping mass of precursor and fragment ion from SILAC labeling were corrected by specific ions (y1, y3, or y4 ions).

Estimation of NMDERCs by ODE. Data from the first four time points were taken to estimate rate constants. A total of 44 NMDERCs were estimated by solving 84 ODE equations by using ODE45 solver (version 7.10; Matlab) with code reported previously (20) and adapted to the kinetic scheme of Fig. S4.

ACKNOWLEDGMENTS. This work was supported by Northwestern University, the Chicago Biomedical Consortium with support from the Searle Funds at the Chicago Community Trust, a gift from the Zell Family to the Robert H. Lurie Comprehensive Cancer Center, National Institutes of Health Grants R01 GM 067193-09 (to N.L.K.) and R01 CA123204 (to J.D.L.), a Leukemia and Lymphoma Society Specialized Center of Research Grant (to J.D.L.), Ruth Kirschstein National Research Service Award F32HL099177 (to R.P.), a fellowship from the European Hematology Association (to E.M.-G.), and Northwestern University Physical Sciences Oncology Center Grant U54 CA 143869.

- Mosammaparast N, Shi Y (2010) Reversal of histone methylation: Biochemical and molecular mechanisms of histone demethylases. *Annu Rev Biochem* 79:155–179.
- Krivtsov AV, Armstrong SA (2007) MLL translocations, histone modifications and leukaemia stem-cell development. *Nat Rev Cancer* 7:823–833.
- Martinez-Garcia E, et al. (2011) The MMSET histone methyl transferase switches global histone methylation and alters gene expression in t(4;14) multiple myeloma cells. *Blood* 117:211–220.
- Morin RD, et al. (2010) Somatic mutations altering EZH2 (Tyr641) in follicular and diffuse large B-cell lymphomas of germinal-center origin. *Nat Genet* 42:181–185.
- Wang Z, et al. (2008) Combinatorial patterns of histone acetylations and methylations in the human genome. *Nat Genet* 40:897–903.
- Barski A, et al. (2007) High-resolution profiling of histone methylations in the human genome. *Cell* 129:823–837.
- Ernst J, et al. (2011) Mapping and analysis of chromatin state dynamics in nine human cell types. *Nature* 473:43–49.
- Martin C, Zhang Y (2007) Mechanisms of epigenetic inheritance. *Curr Opin Cell Biol* 19:266–272.
- Zhu B, Reinberg D (2011) Epigenetic inheritance: Uncontested? *Cell Res* 21:435–441.
- Wagner EJ, Carpenter PB (2012) Understanding the language of Lys36 methylation at histone H3. *Nat Rev Mol Cell Biol* 13:115–126.
- Li Y, et al. (2009) The target of the NSD family of histone lysine methyltransferases depends on the nature of the substrate. *J Biol Chem* 284:34283–34295.
- Margueron R, et al. (2009) Role of the polycomb protein EED in the propagation of repressive histone marks. *Nature* 461:762–767.
- Schmitges FW, et al. (2011) Histone methylation by PRC2 is inhibited by active chromatin marks. *Mol Cell* 42:330–341.
- Sneeringer CJ, et al. (2010) Coordinated activities of wild-type plus mutant EZH2 drive tumor-associated hypertrimethylation of lysine 27 on histone H3 (H3K27) in human B-cell lymphomas. *Proc Natl Acad Sci USA* 107:20980–20985.
- Marango J, et al. (2008) The MMSET protein is a histone methyltransferase with characteristics of a transcriptional corepressor. *Blood* 111:3145–3154.
- Lauring J, et al. (2008) The multiple myeloma associated MMSET gene contributes to cellular adhesion, clonogenic growth, and tumorigenicity. *Blood* 111:856–864.
- Bonenfant D, et al. (2007) Analysis of dynamic changes in post-translational modifications of human histones during cell cycle by mass spectrometry. *Mol Cell Proteomics* 6:1917–1932.
- Scharf AN, Barth TK, Imhof A (2009) Establishment of histone modifications after chromatin assembly. *Nucleic Acids Res* 37:5032–5040.
- Sweet SM, Li M, Thomas PM, Durbin KR, Kelleher NL (2010) Kinetics of re-establishing H3K79 methylation marks in global human chromatin. *J Biol Chem* 285:32778–32786.
- Zee BM, et al. (2010) In vivo residue-specific histone methylation dynamics. *J Biol Chem* 285:3341–3350.
- Jenuwein T, Allis CD (2001) Translating the histone code. *Science* 293:1074–1080.
- Strahl BD, Allis CD (2000) The language of covalent histone modifications. *Nature* 403:41–45.
- Yuan W, et al. (2011) H3K36 methylation antagonizes PRC2-mediated H3K27 methylation. *J Biol Chem* 286:7983–7989.
- Zee BM, Levin RS, Dimaggio PA, Garcia BA (2010) Global turnover of histone post-translational modifications and variants in human cells. *Epigenetics Chromatin* 3:22.
- Wolf-Yadlin A, Hautaniemi S, Lauffenburger DA, White FM (2007) Multiple reaction monitoring for robust quantitative proteomic analysis of cellular signaling networks. *Proc Natl Acad Sci USA* 104:5860–5865.
- Darwanto A, et al. (2010) A modified “cross-talk” between histone H2B Lys-120 ubiquitination and H3 Lys-79 methylation. *J Biol Chem* 285:21868–21876.
- Drogaris P, et al. (2009) Enhanced protein detection using a trapping mode on a hybrid quadrupole linear ion trap (Q-Trap). *Anal Chem* 81:6300–6309.
- FitzGerald J, et al. (2011) Regulation of the DNA damage response and gene expression by the Dot1L histone methyltransferase and the 53Bp1 tumour suppressor. *PLoS ONE* 6:e17414.
- Veenstra TD, Martinović S, Anderson GA, Pasa-Tolić L, Smith RD (2000) Proteome analysis using selective incorporation of isotopically labeled amino acids. *J Am Soc Mass Spectrom* 11:78–82.
- Kuo AJ, et al. (2011) NSD2 links dimethylation of histone H3 at lysine 36 to oncogenic programming. *Mol Cell* 44:609–620.
- McCabe MT, et al. (2012) Mutation of A677 in histone methyltransferase EZH2 in human B-cell lymphoma promotes hypertrimethylation of histone H3 on lysine 27 (H3K27). *Proc Natl Acad Sci USA* 109:2989–2994.
- Garcia BA, Pesavento JJ, Mizzen CA, Kelleher NL (2007) Pervasive combinatorial modification of histone H3 in human cells. *Nat Methods* 4:487–489.
- Phanstiel D, et al. (2008) Mass spectrometry identifies and quantifies 74 unique histone H4 isoforms in differentiating human embryonic stem cells. *Proc Natl Acad Sci USA* 105:4093–4098.
- Garcia BA, et al. (2007) Chemical derivatization of histones for facilitated analysis by mass spectrometry. *Nat Protoc* 2:933–938.
- MacLean B, et al. (2010) Skyline: an open source document editor for creating and analyzing targeted proteomics experiments. *Bioinformatics* 26:966–968.